High-Pressure Polymerization of Ethylene in Tubular Reactors: A Rigorous Dynamic Model Able to Predict the Full Molecular Weight Distribution

Mariano Asteasuain,* Adriana Brandolin

A rigorous dynamic model of the high-pressure polymerization of ethylene in tubular reactors is presented. The model is capable of predicting the full molecular weight distribution (MWD), average branching indexes, monomer conversion and average molecular weights as function of time and reactor length. The probability generating function method is applied to model the MWD. This technique allows easy and efficient calculation of the MWD, in spite of the complex mathematical description of the process. The reactor model is used to analyze the dynamic responses of MWD and other process variables under different transition policies, as well as to predict the effects of process perturbations. The influence of the material recycle on the process dynamics is also shown.

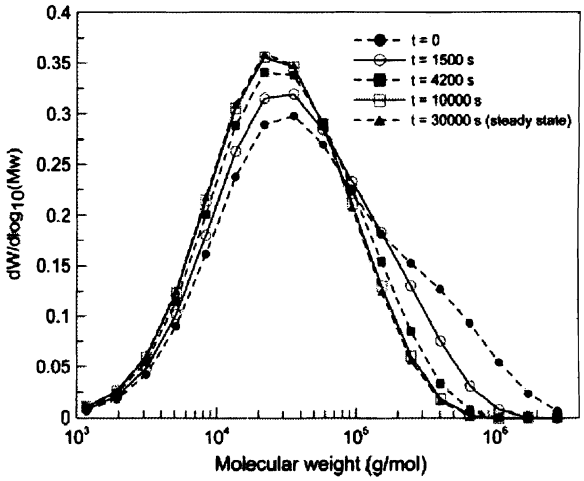

Introduction

The high-pressure polymerization of ethylene in tubular reactors is a widely employed industrial process. It allows branched low-density polyethylene (LDPE) to be obtained with characteristics that have not been reproduced by more modern low- or medium-pressure polymerizations. The process is carried out under rigorous conditions. For instance, the reactor is operated at very high pressure, between 1 300 and 3 000 bar at the inlet. The temperature rises from about 50 °C at the reactor inlet to 330 °C at the hottest points due to the exothermic polymerization. Axial velocities are also high, usually around $10\,m \cdot s^{-1}$. In addition, the reactor configuration is complex. The main feed usually consists of ethylene, inert components, transfer agents to control the molecular weight and, eventually, oxygen as initiator. Most of the polymerization reaction, however, is initiated by peroxides that are fed to the reactor through lateral injections. Monomer and/or transfer agents can also be fed through side injections. The polymerization takes place in short reaction zones following the peroxide injections, exhibiting high heat generation and steep temperature profiles. The remainder of the reactor is mainly used as a heat exchanger, where the reaction mixture is heated or cooled in order to reach appropriate temperatures for peroxide addition or for downstream units. The control of the temperature of the reaction mixture is achieved by circulating vapor or liquid

M. Asteasuain, A. Brandolin
Planta Piloto de Ingeniería Química (Universidad Nacional del Sur – CONICET), Camino La Carrindanga km. 7, 8000 Bahía Blanca, Argentina
Fax: +54-291-4861600; E-mail: masteasuain@plapiqui.edu.ar

Macromol. React. Eng. **2009**, *3*, 398–411

DOI: 10.1002/mren.200900013

water through different jacket zones. These jacket zones are generally independent of each other, or may be interconnected under different configurations; the jacket flow rate can be co- or counter-current. Moreover, some of these reactors are provided with a let-down valve located at the reactor exit that is periodically opened to produce a pressure pulse which sweeps out the polymer from the walls. In addition, the interaction between the different reacting species is very complex, and there is an intricate connection between polymer quality and process conditions.

In this context, a mathematical model is a fundamental tool for the process engineer. It allows the safe and economic study of the influence of different design and operative variables on production and product quality. It is also very valuable for optimizing the process. In order to achieve high-quality results that are useful for actual industrial plants, comprehensive models with accurate predictive capabilities are required. In spite of being a complex task, a considerable amount of research work has been devoted to the mathematical modeling of industrial LDPE tubular reactors. Nowadays, it remains an academic and technological challenge to further understand this process. Rigorous steady-state models of this process have been reported in the literature.[1–5] In general, these models consider realistic reactor configurations and include detailed predictions of physical and transport properties along the axial distance. Several applications of parametric analysis,[6] optimization studies[7–13] and parameter estimation techniques[4,5,14] have been reported. Most models have focused on polymer average molecular properties, like the average molecular weights or average degrees of branching. However, attempts to predict distributions, such as the full molecular weight distribution (MWD) or two-dimensional distributions in molecular weight and branching frequency have also been reported.[9,15,16]

On the other hand, less attention has been devoted to the dynamic operation of these reactors. Dynamics is an important component of the performance of this process. As is usual in continuous polymerization plants, different polymer grades are produced in the same equipment. Therefore, normal operation requires changes from one steady state to another, in order to switch among different final products. In the transient states during these changes, off-specification, low-value product is generally produced. Besides, these reactors are commonly connected in production networks. Changes in upstream or downstream processes may modify the reactor throughput, causing disturbances that affect the polymer quality properties. Dynamic operation is also important in start-up or shut-down procedures. In order to cope efficiently with all these scenarios, detailed dynamic models that provide accurate information about the process are necessary. Although it has been stated that a quasi-steady-state can be assumed in this process,[11] recent works have shown that the dynamics cannot be ignored under certain conditions, specially when material recycling is involved.[17] There are few works dealing with the dynamic operation of this process available in the literature. In general, strong simplifications have been applied in order to reduce the high model complexity of this system. For instance, Asteasuain et al.[18] developed a dynamic model that assumed piecewise constant profiles for the physical and transport properties, and considered a reduced kinetic mechanism, allowing prediction of only some of the major quality properties of the polymer. The model was successfully used in optimization studies to obtain optimal start-up strategies that improved reactor productivity while keeping the predicted molecular properties within commercial ranges. A similar model was employed by Cervantes et al.[19] as the reactor module of a dynamic model of a LDPE plant. They performed a large-scale optimization of the whole polyethylene plant and obtained optimal control policies for the feed streams that minimized the transient states generated during grade transitions.

A few dynamic models involving a more comprehensive description of the process have been reported. Häfele et al.[17] developed a mathematical model describing a plant for the production of LDPE, including a detailed reactor model. This model consisted of partial differential equations in time and space for the mass balances of the components of the reaction mixture and MWD moments, based on a complete kinetic mechanism, energy balances for the reaction mixture, reactor wall and reactor jackets, and detailed correlations for the calculation of physical and transport properties. Using this model, they studied the plant dynamics, including the influence of the reactor wall and of the material recycle. They concluded that the reactor wall plays an important role in the dynamic behavior of the reactor and that the material recycle increases significantly the time constant of the process, from minutes to hours. Mummudy and Fox[20] developed a comprehensive model of the tubular LDPE reactor. They used a two-environment model to describe micromixing at the initiator injection points, and included a model for pressure-pulsing due to let-down valve operation. They analyzed operation conditions that could lead to reactor runaway due to ethylene decomposition. Zavala and Biegler[21] employed a comprehensive dynamic model of the LDPE in a moving horizon estimation (MHE) application for inferring model states and critical uncertain time-varying phenomena, such as reactor fouling, in space and time. The reactor model assumed the quasi-steady-state for the mass and energy balances inside the reactor based on the fast dynamics of the reaction mixture, but time-dependent energy balances for the reactor wall and the countercurrent jackets were considered. In spite of the large scale of the mathematical model, the MHE exhibited fast response, which made it appropriate for industrial applications.

The models employed in these previous contributions regarding dynamic operation of the LDPE reactor predicted only average molecular properties. None of them attempted to model the complete MWD of the polymer. In previous works, we have developed a rigorous steady state model of a LDPE tubular reactor.[9,22] This model was validated against experimental data from an actual industrial reactor. In this work, we present an extension of that model, consisting of the incorporation of the process dynamics. The comprehensiveness of the former model has been kept. This involves employing rigorous correlations for the calculation of physical and transport properties, such as density, viscosity and heat capacity of the reaction mixture and coolant, as well as the heat-transfer coefficient, along the axial distance and time. A realistic reactor configuration, for example, including side feeds and multiple jacket zones, is also considered. The resulting model is capable of predicting the full MWD, as well as average branching indexes, monomer conversion and average molecular weights as a function of time and reactor length. This model is used to study the influence of different dynamic scenarios on process and product quality variables. Grade transition policies are also analyzed.

Process Description and Mathematical Model

A simplified flow sheet of the LDPE process analyzed in this work is displayed in Figure 1. The polymer is produced by the high-pressure polymerization of ethylene in a tubular reactor, using oxygen and peroxide mixtures as initiators. The make-up stream, consisting of ethylene, inert components, oxygen and transfer agents, is mixed with the low-pressure recycle stream. Afterwards, it is compressed to about 250 bar in a multi-stage primary compressor. This stream is mixed with the high-pressure recycle stream, and then compressed in a hyper-compressor up to the reaction pressure, which is usually around 2 000–2 800 bar. The compressor outlet is fed to the jacketed tubular reactor, where the ethylene is polymerized with a conversion per pass of approximately 25–30%. Although the reaction is partially initiated by oxygen, most of the polymerization is initiated by organic peroxide mixtures. These peroxides are added at additional feed points located at different axial positions, producing short reaction zones with sharp increases of temperature and conversion. The remaining reactor zones are mainly used as heat exchangers in order to reach appropriate temperatures for peroxide addition or for downstream units. Monomer and/or transfer agents can also be fed through side feeds. The control of the reactor temperature is achieved by circulating vapor or liquid water through independent tube jackets. The reactor output is expanded in a let-down valve, which produces a pressure pulse that travels back along the reactor removing polymer build ups from the reactor wall. The expanded reactor output is separated first in a high-pressure separator and then in a low-pressure one. Unreacted ethylene and transfer agents, and inert components, are cooled and then recycled. The polymer is obtained from the low-pressure separator. The particular configuration of the reactor analyzed in this work considers eight jacket zones and two lateral feeds.

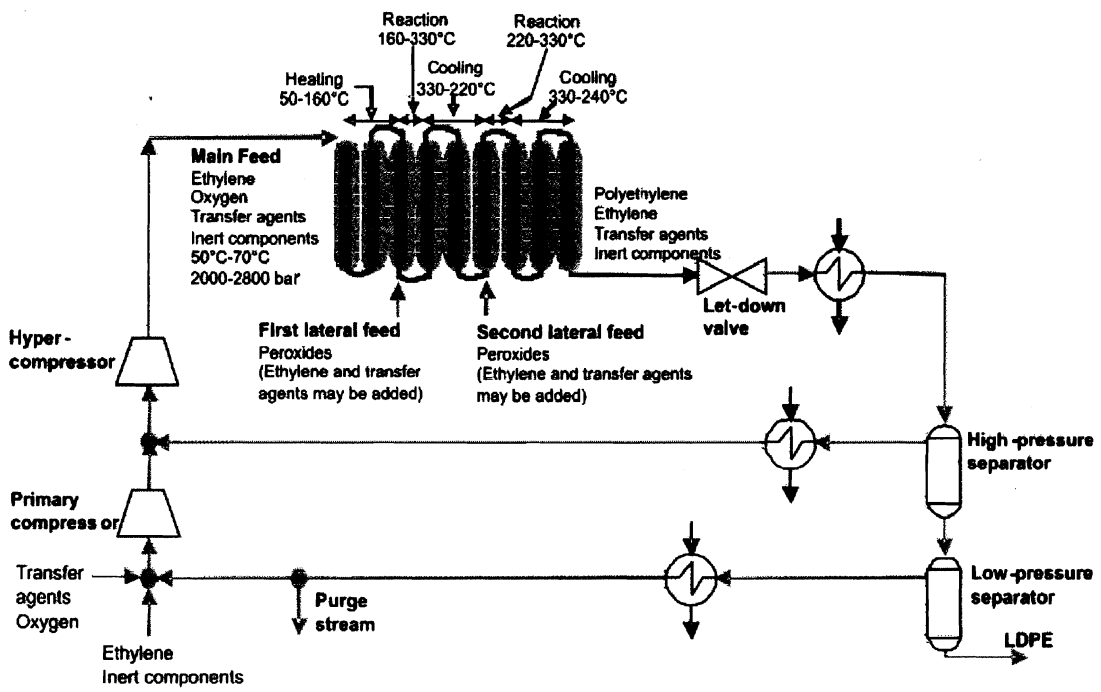

Figure 1. Simplified flow sheet of the LDPE production plant.

Macromol. React. Eng. **2009**, *3*, 398–411

DOI: 10.1002/mren.200900013

Table 1. Kinetic mechanism.

Step	Equation
Peroxide initiation	$I_k \xrightarrow{f_{ik},k_{ik}} 2R(0) \quad k=1,2$ (1)
Monomer thermal initiation	$3M \xrightarrow{k_{mi}} R(1)+R(2)$ (2)
Propagation	$R(m)+M \xrightarrow{k_p} R(m+1)$ (3)
Thermal degradation	$R(m) \xrightarrow{k_{tdt}} P(m)+R(0)$ (4)
Chain transfer to polymer	$R(n)+P(m) \xrightarrow{m k_{trp}} P(n)+R(m)$ (5)
Backbiting	$R(m) \xrightarrow{k_{bb}} R(m)$ (6)
β-Scission of tertiary radical	$R(m) \xrightarrow{k_\beta} P(m)+R(0)$ (7)
Oxygen initiation	$O_2+M \xrightarrow{k_o} 2R(0)$ (8)
Generation of inert	$O_2+R(m) \xrightarrow{f_o k_o} X$ (9)
Termination by combination	$R(n)+R(m) \xrightarrow{k_{tc}} P(n+m)$ (10)
Chain transfer to monomer	$R(m)+M \xrightarrow{k_{trm}} P(m)+R(1)$ (11)
Chain transfer to transfer agent	$R(m)+S \xrightarrow{k_{trs}} P(m)+R(0)$ (12)
β-Scission of secondary radical	$R(m) \xrightarrow{k_{\beta 1}} P(m)+R(0)$ (13)

This work is focused on the analysis of the tubular reactor unit. The mathematical model of the polymerization reactor is based on a previous, comprehensive steady-state model developed by the authors,[9,22] which is extended by incorporating the process dynamics. The model assumes plug flow and supercritical reaction mixture. It also considers variation of physical and transport properties (i.e., axial velocity, heat capacity, thermal conductivity, viscosity and density) along the axial distance, calculated with rigorous correlations. Detailed calculations of heat-transfer coefficient profiles are also made.[3] The kinetic mechanism considered in the reactor model is shown in Table 1. It includes all the kinetic steps commonly proposed in the literature for this process. In order to avoid iterative calculations that increase the computational burden, the jacket temperature at each one of the eight reaction zones is assumed to be uniform, and the pressure pulse is neglected. The peroxide and transfer agent mixtures are treated as a single fictitious species. These simplifications were validated in a previous work by the authors[22] against several data sets from an industrial tubular reactor. The same transfer agent mixture, and therefore the same single fictitious transfer agent (S), that is employed for the main reactor feed is considered for possible lateral feeds. However, peroxide mixtures for the first and second lateral feeds are different in composition,[22] and hence, they are represented in this model by two different fictitious peroxides (I_1 for the first lateral feed and I_2 for the second one). The set of kinetic constants reported by Asteasuain et al.[22] is used here. These constants are considered to follow an Arrhenius equation. Their frequency factors and activation energies were determined in that work by a least-squares minimization procedure against several data sets from an actual industrial reactor. The conventional Arrhenius equation was used in that work, without reparameterization in terms of a reference temperature. The model parameters involved in this fitting also included the efficiencies of the fictitious initiators, which are regarded as fixed model parameters.

The main model equations are outlined in Table 2. The well-known method of moments and the probability generating function (pgf) transformation technique[23,24] are employed for calculating the average molecular weights and the full MWD, respectively. Both techniques start from the theoretically infinite mass balances of macroradicals and dead polymer of all possible chain lengths that may be present in the reaction mixture [$R(m)$ and $P(m)$, respectively, in Table 1, where $m=0,\ldots,\infty$]. The method of moments applies a transformation of these balances, leading to balance equations for the ath order moments of the macroradical and polymer MWD (λ_a and μ_a, respectively). These moments are used to compute the average molecular weights according to Equation (16) and (17). Expressions for the macroradicals and polymer balance equations and for reaction rates of the MWD moments can be found elsewhere.[9]

Table 2. Outline of the main model equations.

Description	Equation
Global mass balance	$\frac{\partial(\rho(z,t)\,v(z,t))}{\partial z}+\frac{\partial\rho(z,t)}{\partial t}=0$ (14)
Pressure drop	$\frac{\partial P(z,t)}{\partial z}=c$ c : constant parameter (15)
Number average molecular weight	$\mathrm{Mn(z,t)}=\mathrm{Mw_M}\frac{\lambda_1(z,t)+\mu_1(z,t)}{\lambda_0(z,t)+\mu_0(z,t)}$ (16)
Weight average molecular weight	$\mathrm{Mw(z,t)}=\mathrm{Mw_M}\frac{\lambda_2(z,t)+\mu_2(z,t)}{\lambda_1(z,t)+\mu_1(z,t)}$ (17)
Short chain branches/1000 C	$\mathrm{SCB/1000C}(z,t)=500\frac{\mathrm{Me}(z,t)}{\lambda_1(z,t)+\mu_1(z,t)}$ (18)
Full MWDs	$n_i(z,t)=f(\phi_0(z,t),\varphi_0(z,t),\lambda_0(z,t),\mu_0(z,t))$ $w_i(z,t)=f(\phi_1(z,t),\varphi_1(z,t),\lambda_1(z,t),\mu_1(z,t))$ $\left(\frac{dW}{d(\log_{10}Mw)}\right)_i(z,t)=f(\phi_2(z,t),\varphi_2(z,t),\lambda_1(z,t),\mu_1(z,t))$ $n_i(z,t)$: number fraction distribution $w_i(z,t)$: weight fraction distribution $\left(\frac{dW}{d\log_{10}Mw}\right)_i(z,t)$: differential log distribution $f(.)$: algebraic equations of the pgf inversion algorithm i: chain length (19)
Mass balances of components, MWD moments and pgfs	$\frac{\partial C_j(z,t)}{\partial t}+\frac{\partial v(z,t)C_j(z,t)}{\partial z}=r_j(z,t)$ $j=O_2$(oxigen), M(ethylene), I_k(kth initiator, $k=1,2$), S(transfer agent), Me (methyl groups), Vi (vinyl groups), Vd (vinylidene groups), LCB (long chain branches), λ_a(ath order moment of the macroradical MWD, $a=0,1,2$), μ_a(ath order moment of the dead polymer MWD, $a=0,1,2$), $\lambda_a\cdot\phi_{a,l}$(product of the ath moment times the ath pgf transform of the macroradical MWD, $a=0,1,2$,l : dummy variable), $\mu_a\cdot\varphi_{a,l}$(product of the ath moment times the ath pgf transform of the dead polymer MWD, $a=0,1,2$,l : dummy variable) (20)
Energy balance	$\cdot\rho(z,t)\,\mathrm{Cp}(z,t)\frac{\partial T(z,t)}{\partial t}+\rho(z,t)\,v(z,t)\mathrm{Cp}(z,t)\frac{\partial T(z,t)}{\partial z}=-\frac{4U(z,t)(T(z,t)-T_j)}{D}+r_{\mathrm{pm}}(z,t)(-\Delta H)$ (21)
Vinyl groups/1 000 C	$\mathrm{Vi/1000C}(z,t)=500\frac{\mathrm{Vi}(z,t)}{\lambda_1(z,t)+\mu_1(z,t)}$ (22)
Vinylidene groups/1 000 C	$\mathrm{Vd/1000C}(z,t)=500\frac{\mathrm{Vd}(z,t)}{\lambda_1(z,t)+\mu_1(z,t)}$ (23)
Long chain branches/1 000 C	$\mathrm{LCB/1000C}(z,t)=500\frac{\mathrm{LCB}(z,t)}{\lambda_1(z,t)+\mu_1(z,t)}$ (24)

The pgf method consists in a transformation of the macroradicals and polymer balance equations into the pgf transform domain, leading to a finite set of equations where the dependent variables are the pgf transforms of the macroradicals and polymer MWDs ($\phi_{a,l}$ and $\varphi_{a,l}$, respectively). The pgfs calculated by solving the transformed equations are then inverted to recover the MWDs. Three types of pgf were defined, distinguished by subscript a, as shown in Equation (25) and (26)

$$\phi_{a,l}=\sum_{n=1}^{\infty}l^n\frac{n^aR(m)}{\lambda_a} \quad (25)$$

$$\varphi_{a,l}=\sum_{n=1}^{\infty}l^n\frac{n^aP(m)}{\mu_a} \quad (26)$$

where $a=0$, 1, 2. These pgfs represent the transforms of the MWD expressed as number fraction versus molecular weight (n_i) when $a=0$, weight fraction versus molecular

Macromol. React. Eng. **2009**, *3*, 398–411

Macromolecular Journals
DOI: 10.1002/mren.200900013

Table 3. pgf reaction rates and Stehfest inversion algorithm.

Description	Equation
*a*th pgf transform of the macroradical MWD, *a* = 0, 1, 2	$\hat{r}_{\phi_{a,l}=\lambda_a\phi_{a,l}}(z,t) = k_o(z,t)C_{O_2}(z,t)^{1.1}C_M(z,t)\delta_{a,0} + 2f_{i1}k_{i1}(z,t)C_{I_1}(z,t)\delta_{a,0} + 2f_{i2}k_{i2}(z,t)C_{I_2}(z,t)\delta_{a,0}$ $+k_p(z,t)C_M(z,t)l\sum_{j=0}^{a}\binom{a}{j}\hat{C}_{\phi_{j,l}}(z,t) - k_p(z,t)C_M(z,t)\hat{C}_{\phi_{a,l}}(z,t) + (k_{tdt}(z,t) + k_{\beta 1}(z,t)$ $+k_\beta(z,t))C_{\lambda_0}(z,t)\delta_{a,0} + k_{trs}(z,t)C_S(z,t)C_{\lambda_0}(z,t)\delta_{a,0} + k_{trm}(z,t)C_M(z,t)C_{\lambda_0}(z,t)l$ $-k_{tc}(z,t)C_{\lambda_0}(z,t)\hat{C}_{\phi_{a,l}}(z,t) - (k_{tdt}(z,t) + k_{\beta 1}(z,t) + k_\beta(z,t))\hat{C}_{\phi_{a,l}}(z,t)$ $-k_{trs}(z,t)C_S(z,t)\hat{C}_{\phi_{a,l}}(z,t) - k_{trm}(z,t)C_M(z,t)\hat{C}_{\phi_{a,l}}(z,t) + k_{ini}(z,t)C_M(z,t)^3(l + 2^a l^2)$ $-f_o k_o(z,t)C_{O_2}(z,t)^{1.1}\hat{C}_{\phi_{a,l}}(z,t) - k_{trp}(z,t)C_{\mu_1}(z,t)\hat{C}_{\phi_{a,l}}(z,t) + k_{trp}(z,t)C_{\lambda_0}(z,t)\hat{C}_{\varphi_{a+1,l}}(z,t)$ (27)
*a*th pgf transform of the polymer MWD, a = 0, 1, 2	$\hat{r}_{\varphi_{a,l}=\mu_a\varphi_{a,l}}(z,t) = \frac{1}{2}k_{tc}(z,t)\sum_{j=0}^{a}\binom{a}{j}\hat{C}_{\phi_{j,l}}(z,t)\hat{C}_{\phi_{a-j,l}}(z,t) + (k_{tdt}(z,t) + k_{\beta 1}(z,t)$ $+k_\beta(z,t))\hat{C}_{\phi_{a,l}}(z,t) + k_{trp}(z,t)C_{\mu_1}(z,t)\hat{C}_{\phi_{a,l}}(z,t) - k_{trp}(z,t)C_{\lambda_0}(z,t)\hat{C}_{\varphi_{a+1,l}}(z,t)$ $+k_{trm}(z,t)C_M(z,t)\hat{C}_{\phi_{a,l}}(z,t) + k_{trs}(z,t)C_S(z,t)\hat{C}_{\phi_{a,l}}(z,t)$ (28)
Closure technique for $\varphi_{3,l}$[26]	$\hat{C}_{\varphi_{3,l}}(z,t) = \frac{\hat{C}_{\varphi_{2,l}}(z,t)^2}{\hat{C}_{\varphi_{1,l}}(z,t)} + \hat{C}_{\varphi_{2,l}}(z,t) - \hat{C}_{\varphi_{1,l}}(z,t)$ (29)
Stehfest inversion algorithm	$d_{a,i}(z,t) = \frac{\ln(2)}{i}\sum_{j=1}^{J}A_j\frac{(\phi_{a,l}(z,t) + \varphi_{a,l}(z,t))}{\lambda_b(z,t) + \mu_b(z,t)}$ $l = e^{-j\ln(2)/i}$, $b = a$ *if* $a = 0$ or 1, $b = 1$ *if* $a = 2$, $a = 0,1,2$
	$A_j = (-1)^{j+J/2}\sum_{m=[(j+1)/2]}^{\min(j,J/2)}\frac{m^{J/2}(2m)!}{(J/2-m)!m!(m-1)!(j-m)!(2m-j)!}$ (30)
	where $d_{0,i}=n_i$, $d_{1,i}=w_i$, $d_{2,i}=(dW/d\log_{10}\overline{M}_w)_i$

weight (w_i) when $a = 1$ and the product of weight fraction and molecular weight versus molecular weight [used to calculate the differential log distribution, $(dW/d\log_{10}\overline{M}_w)_i$] when $a = 2$. Inversion of each type of pgf allows the recovery of the three kinds of distribution independently, thereby attenuating numerical noise propagation.[25] Tedious algebraic operations needed for the transformation of the mass balances can be avoided by using of the pgf transform table we previously developed.[23] The resulting terms for the reaction rates r_j in Equation (20) in Table 2, with $j = \lambda_a \cdot \phi_{a,l}$ and $\mu_a \cdot \varphi_{a,l}$, are shown in Table 3. The pgf inversion algorithm employed in this model is the adaptation of the Stehfest algorithm for pgf inversion.[25] The equations corresponding to this inversion algorithm [represented by function $f(.)$ in Table 2] are also shown in Table 3. The pgf technique allowed the MWD to be modeled easily and efficiently, in spite of the reactor model complexity.

Rigorous correlations validated against industrial data were proposed in previous steady-state versions of the model for the prediction of physical and transport properties.[1,3,27] These correlations are shown in Table 4. Equation (31) corresponds to the overall heat-transfer coefficient ($U(z,t)$) between the reaction mixture and the jacket fluid. The overall resistance to heat transfer is formed by the sum of four terms: the film resistance at the reaction mixture side (1st term), thermal resistance through the reactor wall (2nd term), film resistance at the jacket side (3rd term) and fouling resistance (4th term). In Lacunza et al.,[3] particular expressions were developed for the inside film transfer coefficient in terms of concentrations, velocities and thermodynamic properties of the reaction mixture for laminar, transition and turbulent flow regimes, which may be all present along the tubular reactor. These expressions consisted of appropriate modifications to conventional heat exchanger design correlations, taking into account the particular features of this system, such as the influence of the molecular weight of the polymer. A mechanism was also specially developed for the fouling pattern in the reactor. It considers polymer

Table 4. Correlations for physical and transport properties.

Property	Correlation
Overall heat transfer coefficient	$\frac{1}{U(z,t)} = \frac{1}{h_j(z,t)D_e/D} + \frac{2.3D}{2k_w}\log\left(\frac{D_e}{D}\right) + \frac{1}{h_i(z,t)} + R_f(z,t)$ (31)[3]
Monomer density ($g \cdot cm^{-3}$)	$\rho_M(z,t) = (0.6282 - 0.6703 \times 10^{-3}(T(z,t) + 273.15) + 0.1277 \times 10^{-6}(T(z,t) + 273.15)^2 + 0.6799 \times 10^{-4}P(z,t) - 0.1277 \times 10^{-7}P(z,t)^2 + 0.8108 \times 10^{-7}P(z,t)(T(z,t) + 273.15)$ (32)[27]
Polymer density ($g \cdot cm^{-3}$)	$\rho_p(z,t) = \frac{1}{0.949 \times 4.998 \times 10^{-4}(T(z,t) + 273.15)}$ (33)[28]
Reaction mixture density	$\rho(z,t) = \frac{1}{\frac{w_M(z,t) + w_S(z,t) + w_X(z,t)}{\rho_M(z,t)} + \frac{1 - w_M(z,t) - w_S(z,t) - w_X(z,t)}{\rho_P(z,t)}}$ (34)
Reaction mixture viscosity (poise)	$\eta(z,t) = \left(1.98 \times 10^{-4} + 1.15 \times 10^2 (T(z,t) + 273.15)^{-2}\right) 10^{0.0313\mu_1(z,t)^{3/2}\mu_0(z,t)^{-1/2}}$ (35)[28]
Monomer specific heat ($cal \cdot g^{-1} \cdot K^{-1}$)	$Cp_M(z,t) = (0.6919 + 9.838 \times 10^{-4}(T(z,t) + 273.15) - 8.84 \times 10^{-6}P(z,t))/1.8$ (36)
Polymer specific heat ($cal \cdot g^{-1} \cdot K^{-1}$)	$Cp_p(z,t) = 1.041 + 8.3 \times 10^{-4}(T(z,t) + 273.15)$ (37)[28]
Reaction mixture specific heat	$Cp = Cp_M(w_M + w_S + w_X) + Cp_p(1 - w_M - w_S - w_X)$ (38)
Thermal conductivity ($cal \cdot cm^{-1} \cdot s^{-1} \cdot K^{-1}$)	$k = 5 \times 10^{-4}w_M + 3.5 \times 10^{-4}(1 - w_M)$ (39)[28]

deposition and removal rates, resulting in an algebraic expression that computes the fouling resistance along the reactor [$R_f(z,t)$] at a given time as function of monomer conversion, monomer and radical concentrations and reaction mixture density. The model for the overall heat-transfer coefficient was adjusted to fit experimental heat-transfer data from an actual industrial reactor. For the sake of brevity, the whole set of expressions is not included here, but can be found elsewhere, together with details of their derivation.[3] The monomer density, Equation (32), is represented by a quadratic polynomial function of temperature and pressure. The coefficients of these functions were adjusted to fit the Benedict-Webb-Rubbin density predictions.[1] The remaining expressions in Table 4 were developed[1,27] based on those proposed by Chen et al.[28].

Peripheral units, such as compressors, separators and heat exchangers in the recycle section are not modeled because for the scope of this work, only the qualitative effects of the material recycle on the reactor performance are needed. Instead, a perfect separation of the polymer from the remaining components of the reactor output is assumed. The resulting recycle stream and the make-up stream are considered both to be at the reactor feed temperature when they mix with each other. Besides, a pure delay was included in the recycle stream in order to account for the several time delays that are usually present in the separation-recycle section of actual plants.[19]

The process model is then composed by a set of differential algebraic equations (DAE) that are solved simultaneously. These equations are Equation (14–24), (27–39), algebraic equations implicitly included in these, such as the heat transfer coefficients h_j and h_i and fouling term R_f in Equation (31), and auxiliary equations, such as monomer conversion equation and connections between streams. Model implementation was carried out in the commercial software gPROMS (Process Systems Enterprise, Ltd.). A built-in DAE solver that is based on variable time-step/variable order backward differentiation formulae (BDF) was used for the integration of the model equations. For the specific task of computing the coefficients of the Stehfest algorithm [coefficients A_j in Equation (30)], which involve quotients of large factorials with alternating signs, a procedure was developed in FORTRAN code. This code has special built-in functions for calculating the factorials. The FORTRAN procedure was linked to the main gPROMS model using the "foreign object" interface of this software.

Results and Discussion

In order to check the model validity, simulations were performed for different initial conditions. It was observed that model outputs evolved towards the expected steady-

Macromol. React. Eng. **2009**, *3*, 398–411

Macromolecular Journals

DOI: 10.1002/mren.200900013

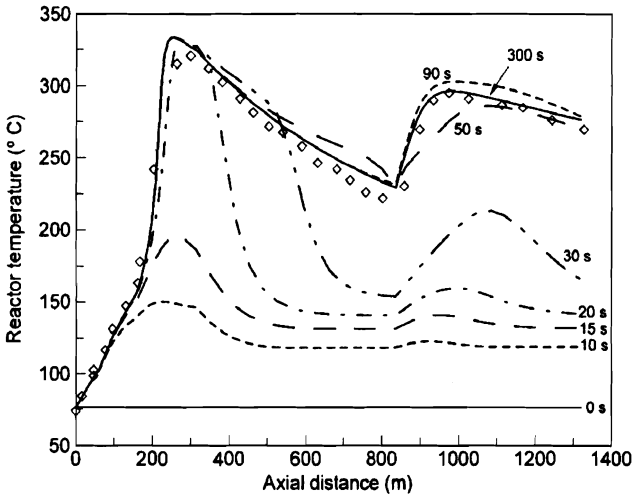

Figure 2. Axial temperature profiles calculated during a reactor start-up. Symbols: plant steady-state values; lines: model.

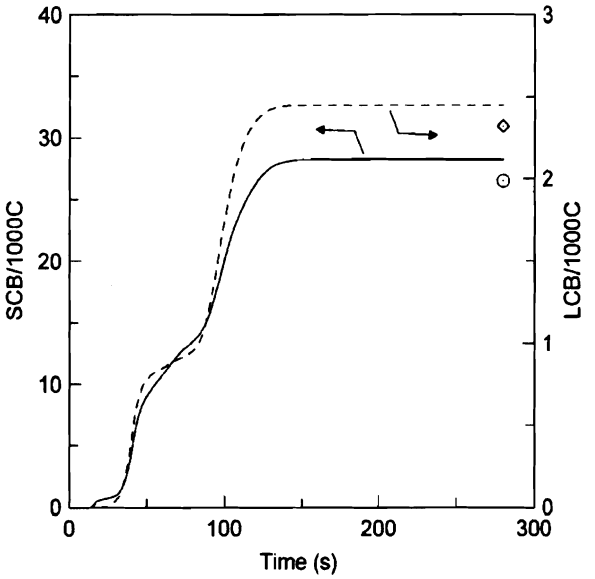

Figure 3. SCB/1000C and LCB/1000C at the reactor exit calculated during a reactor start-up. Symbols: plant steady-state values; lines: model.

state values. Examples of this analysis are presented in Figure 2 and 3. Figure 2 shows the evolution of the temperature profile during a reactor start-up. The reactor is considered to be initially filled with monomer at 76 °C. The recycle stream is disconnected, and operating variables are set at their steady-state values at time 0. It can be observed that the steady-state temperature profile matches the plant data reasonable well. Similar results were obtained for the other major reactor variables. The plant data shown in Figure 2, already reported in previous works by the authors,[18] were measured using a series of thermocouples situated along the tubular reactor, and correspond to a steady-state operating point, the operating conditions of which are listed in Table 5. This steady state will be referred to as the Base Case operating point.

The process simulations employed to obtain the results in Figure 2 and 3 also provide information about the time profiles of the different reactor variables during the start-up. In the case of the reactor temperature profile, for instance, it is interesting to note its extremely rapid increase. The steady-state value of the first temperature peak is reached in 20 s, involving an increment of 255 °C with respect to the initial value. At increasing times, steady-state temperature values along the reactor are reached after an overshoot. However, it can be seen that the temperature value of 345 °C, above which reactor runaway can occur, is never surpassed. Figure 3 shows the time profiles of long- and short-chain branching at the reactor outlet for the same start-up. As expected, both types of chain branching increase with time, since they strongly depend on polymer concentration, which is augmenting at the reactor exit

Table 5. Base Case operating conditions.

Quantity	Value
Inlet temperature (°C)	77
Inlet pressure (bar)	2 300
Oxygen flow rate ($kg \cdot h^{-1}$)	0.25
Transfer agent flow rate ($kg \cdot h^{-1}$)	274
Peroxide flow rate, 1st lateral feed ($kg \cdot h^{-1}$)	3.67
Peroxide flow rate, 2nd lateral feed ($kg \cdot h^{-1}$)	0.57
Monomer flow rate, main feed ($kg \cdot h^{-1}$)	39 600
Monomer flow rate, 1st lateral feed ($kg \cdot h^{-1}$)	0
Monomer flow rate, 2nd lateral feed ($kg \cdot h^{-1}$)	0
Location of 1st lateral feed (z/L)	0.121
Location of 2nd lateral feed (z/L)	0.636
Jacket temperatures, zones 1–8 (°C)	170–225–170–170–170–170–170–170

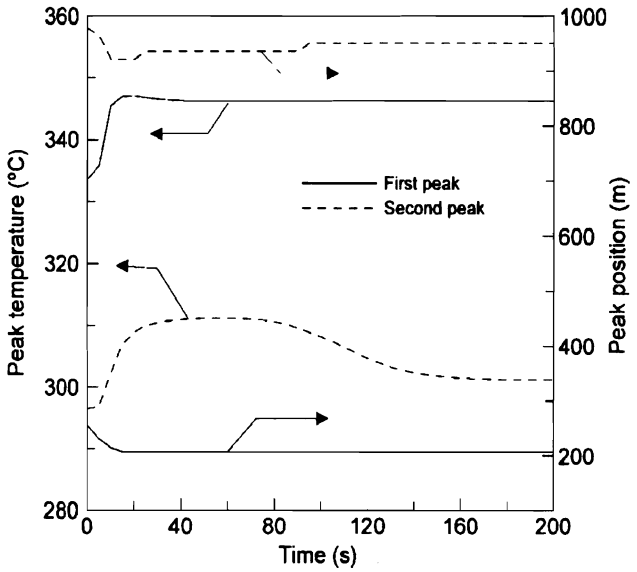

Figure 4. Position and temperature values of the temperature peaks after a step reduction of 30% in the monomer feed rate for the reactor without recycle. The reactor is at the Base Case steady-state point at $t = 0$, when perturbation starts.

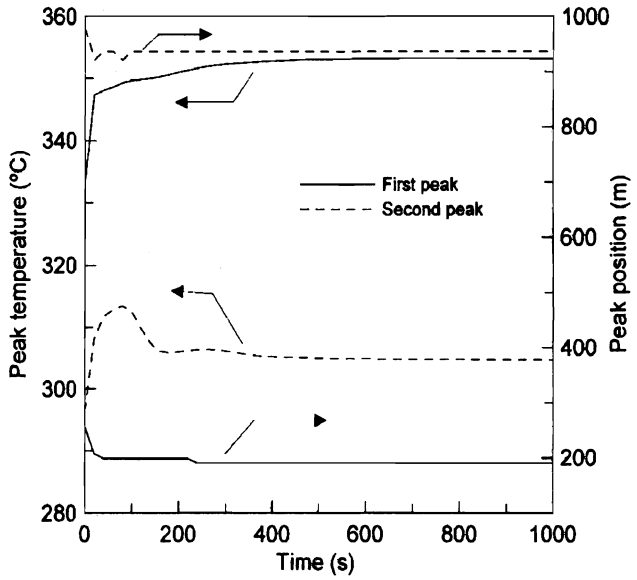

Figure 5. Position and temperature values of the temperature peaks after a step reduction of 30% in the monomer feed rate for the reactor with recycle. The reactor is at the Base Case steady-state point at $t = 0$, when perturbation starts.

because the reactor output corresponds to increasing residence times. It can be seen that two plateaus are present. They are due to the special separation of the two reaction zones.

The model was used to assess the effects of different process perturbations, with and without recycle. Changes in the flow rates of monomer, initiators and transfer agents, as well as in the feed temperature, were analyzed. In order to perform this analysis, the values of these variables at the Base Case were modified by ±20–30%. One of the variables that was found to have a large influence on the process performance was the monomer flow rate. Figure 4 shows the time profiles of the position and temperature values of the temperature peaks after a step reduction of 30% in the monomer feed rate, for the reactor without recycle. Temperature peaks are considered to be very important parameters for the operation of these reactors. It can be seen that the temperature of the first peak surpasses a dangerous value of 345 °C before reaching its steady state-value, and that its position moves towards the reactor entrance. The second peak shows larger differences between its transient and steady-state values. These results show the usefulness of the dynamic model of the process, without which critical information about the condition of the process between steady states would not be available.

Figure 5 shows the time profiles of the temperature peaks for the same perturbation, but for the reactor with recycle. Noting the different time scales of the graphics, it can be seen that the behavior of the second temperature peak with and without recycle are similar. However, the dynamics for the first peak are slower for the reactor with recycle. The time profile of the position of this peak is similar to the one without recycle, but slightly delayed in time. On the contrary, the temperature value of this peak reaches a much higher value than in the previous case, showing a delay in reaching the new steady state of more than ten times longer than before. This slower dynamics is an expected result of the influence of the recycle of material, since the recycle loop needs a time to settle down after the feed perturbation. Consistent results about the influence of the recycle loop on the reactor dynamics have been reported in the literature.[17]

The perturbation consisting of a 30% reduction in the monomer feed with respect to the Base Case causes an important rise in conversion, as shown in Figure 6. This increment is an expected consequence of the increase in the operation temperature. In harmony with temperature profiles, the final conversion is higher when the recycle is active and a longer time is needed for reaching the new steady state. For the reactor with recycle, Figure 7 presents the MWD at the reactor exit during the transient state after the same perturbation. A shift of the MWD to lower molecular weights is observed, which is also consistent with the higher operation temperature. This movement is accompanied by a temporary increase in the peak height. It can also be seen that the time needed for the polymer molecular weight to reach its final state is longer than for reactor performance variables like temperature or conversion. For instance, at time = 1 200 s there is still a difference, particularly in the high molecular weight tail, between the MWD at that time and the final MWD, which is attained approximately 6 000 s after the perturbation in the monomer feed rate took place.

Macromol. React. Eng. **2009**, *3*, 398–411

Macromolecular Journals
DOI: 10.1002/mren.200900013

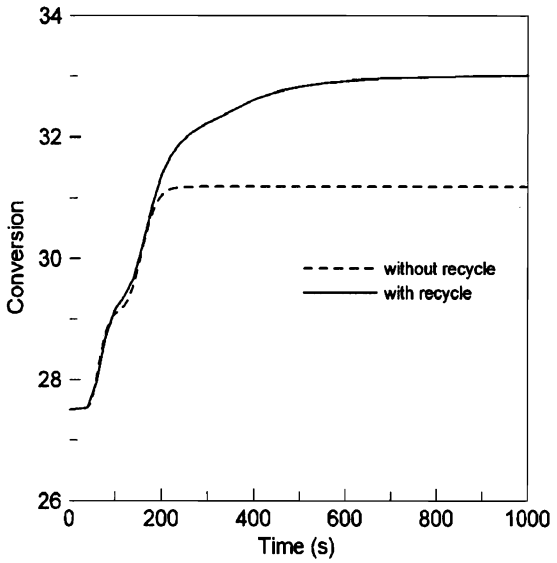

Figure 6. Monomer conversion at the reactor exit after a step reduction of 30% in the monomer feed rate for reactors with and without recycle. The reactor is at the Base Case steady-state point at $t = 0$, when perturbation starts.

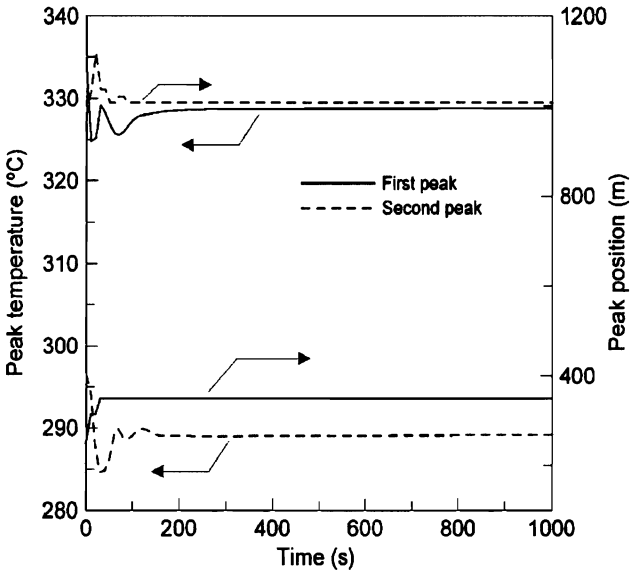

Figure 8. Position and temperature values of the temperature peaks after a step increment of 30% in the monomer feed rate for the reactor with recycle. The reactor is at the Base Case steady-state point at $t = 0$, when perturbation starts.

Figure 8–10 show the process response for a step increment of 30% in the monomer feed rate with respect to the Base Case, for the reactor with recycle. It can be seen in Figure 8 that this perturbation causes a change in the temperature profile that is opposite to the one caused by the 30% reduction in the monomer feed rate (see Figure 5); that is, the temperature peaks shift to the right and their magnitudes decrease. The transient state is shorter than for the monomer feed reduction, in particular for the first temperature peak, and the difference between the initial and final states is considerably smaller. This also holds true for the monomer conversion (Figure 9). However, the positive perturbation in the monomer feed rate significantly affects the polymer molecular weight, causing a broadening of the MWD, as shown in Figure 10. This broadening implies a change in the polydispersity index from 8 to 11. Variation in the MWD is initially faster than for the monomer feed reduction, but the total transition time is similar.

Changes in the transfer agent flow rate also showed a critical impact on the process. This variable stops the growth of the polymer chains by the transfer reaction

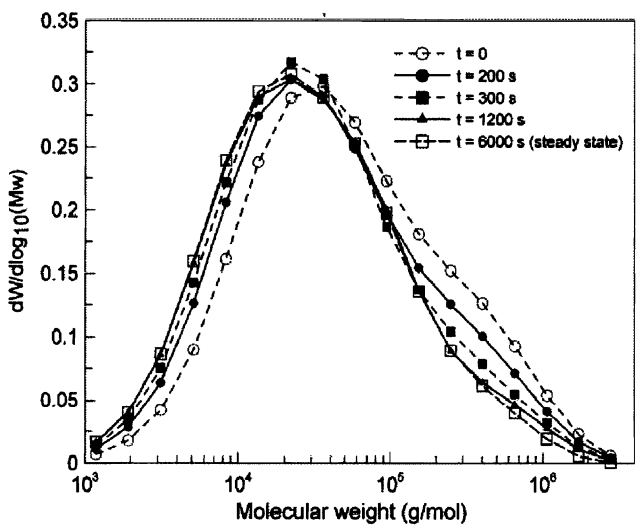

Figure 7. MWD at the reactor exit after a step reduction of 30% in the monomer feed rate for the reactor with recycle. The reactor is at the Base Case steady-state point at $t = 0$, when perturbation starts.

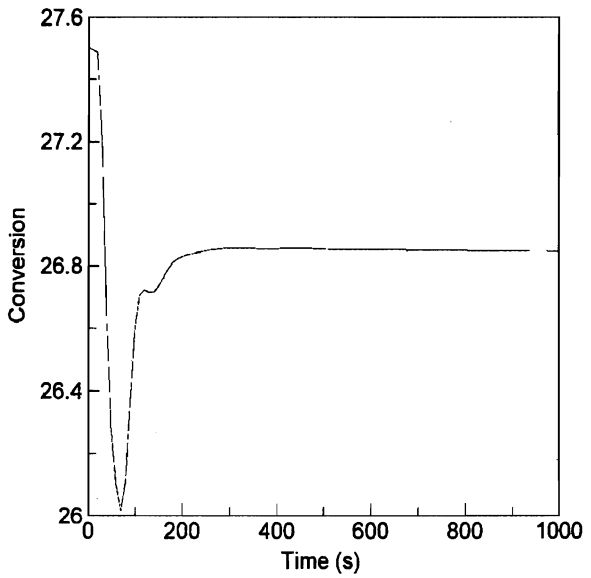

Figure 9. Monomer conversion at the reactor exit after a step increment of 30% in the monomer feed rate for the reactor with recycle. The reactor is at the Base Case steady-state point at $t = 0$, when perturbation starts.

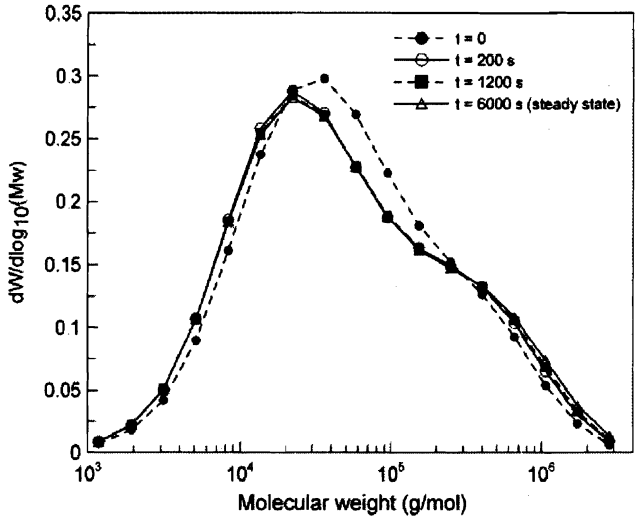

Figure 10. MWD at the reactor exit after a step increment of 30% in the monomer feed rate for the reactor with recycle. The reactor is at the Base Case steady-state point at $t = 0$, when perturbation starts.

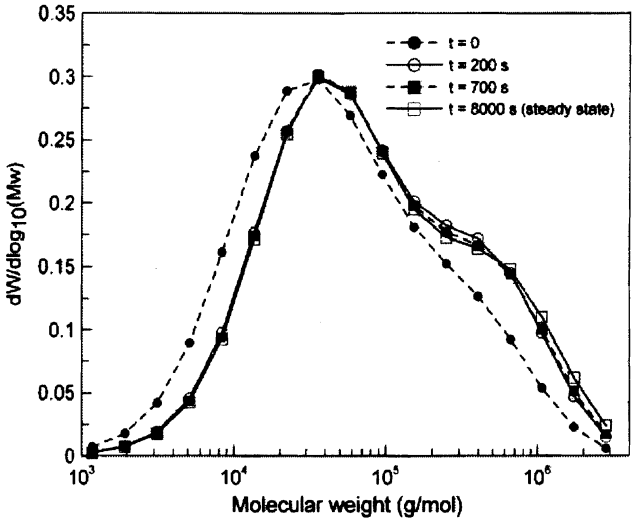

Figure 12. MWD at the reactor exit during grade transition for the reactor with recycle. The reactor is at the Base Case steady-state point at $t = 0$, when the grade transition starts.

shown in Equation (12), reducing the polymer molecular weight. However, as the total number of radicals is not modified by the transfer reaction, its influence on reaction temperature and conversion is not significant in general. Figure 11 shows the MWD after a step increase of 30% in the transfer agent flow rate for the reactor with recycle. As expected, a shift towards lower molecular weights is observed. The magnitude of this shift is very important. For instance, the associated weight average molecular weight decreases by 65%, and the polydispersity index changes from 8 to 4. It should be noticed that dynamics associated with this reactant are particularly slow when the recycle line is connected, as can be seen in the figure. This point will be further discussed later. The remaining variables analyzed, viz., the main feed temperature and the feed rates of the two peroxides, showed negligible influence on the process performance for the magnitude of the perturbations analyzed.

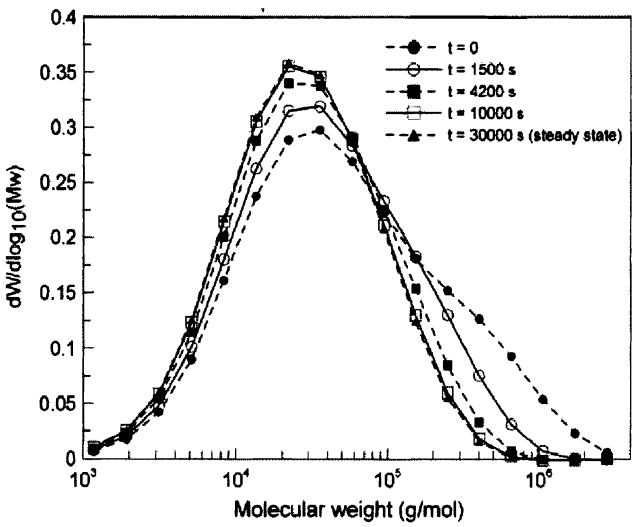

Figure 11. MWD at the reactor exit after a step increment of 30% in the transfer agent feed rate for the reactor with recycle. The reactor is at the Base Case steady-state point at $t = 0$, when perturbation starts.

Transitions between the productions of different polymer grades are frequent and are an important task in the operation of this process. The usual method of achieving these transitions is to modify the transfer agent flow rate,[19] which directly affects the polymer molecular weights as discussed previously. Deviations of the monomer feed to the side feeds may also be applied.[9] Figure 12 shows the evolution of the MWD, considering the reactor without recycle, during a transition from a polyethylene grade of $\overline{M}_w = 140\,000\ g \cdot mol^{-1}$ with a monomodal MWD to a grade of $\overline{M}_w = 220\,000\ g \cdot mol^{-1}$ with a MWD with a high molecular weight shoulder. The new operating scenario involved a reduction of the transfer agent flow rate at the reactor inlet from the Base Case value of 274 to $230\ kg \cdot h^{-1}$, and a diversion of 7% of the monomer feed to the second lateral feed. Also, a different jacket temperature profile was applied. The transition policy consisted of a step change in each of these variables to the operating point value for the new grade. The shift of the MWD to higher molecular weights can be observed in Figure 12. It is interesting to note that the intermediate portion of the MWD partially shifts back to lower molecular weights after a certain time, while the high molecular weight tail of the distribution becomes more important towards the end of the transition, with a marked formation of the shoulder. The grade transition finishes approximately 2.2 h after the change in operating conditions. The detailed tracking of the evolution of the MWD provided by the model has great potential for a careful analysis of transition policies.

Macromol. React. Eng. **2009**, *3*, 398–411

DOI: 10.1002/mren.200900013

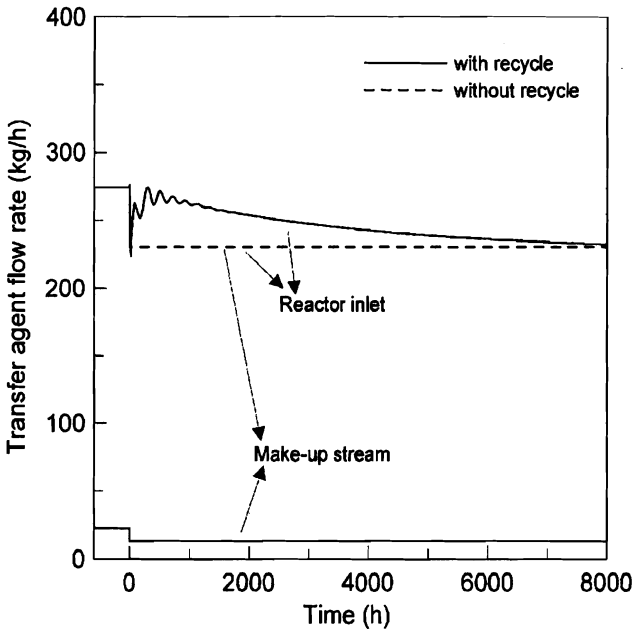

Figure 13. Transfer agent flow rates at the reactor inlet during grade transition for reactors with and without recycle. The reactor is at the Base Case steady-state point at $t = 0$, when make-up flow rates are switched to final values.

The transition time is markedly different for the same transition policy but without material recycle. In this case, the time needed to achieve the transition is only 300 s. This difference may be attributed to the fact that in the no-recycle case the transmission of the change in the make-up stream to the reactor inlet is instantaneous. On the contrary, when the recycle stream is mixed with the make-up stream, the changes in the latter are masked by the return of unreacted monomer and transfer agent. This is particularly important for the transfer agent, because the consumption per pass of this reactant is very small. Hence, a long time is needed before the excess of it is consumed through several passes through the reactor. This is illustrated in Figure 13, which shows the transfer agent flow rate at the reactor inlet and in the make-up stream for the grade transitions with and without recycle. A similar behavior is observed for the monomer flow rate, although the time delay is shorter.

A corollary of these results is that an important benefit can be obtained by optimizing the transition policy. Figure 14 shows the flow rates of transfer agent and monomer at the reactor inlet and in the make-up stream, when the make-up flow rates of monomer and transfer agent were manipulated by PI controllers with the desired flow rates at the reactor inlet as set points. Although the PI controllers had only been roughly tuned by hand, the improvement in transition time was significant. In consequence, the new grade polymer properties are attained in a much shorter time, as can be seen by comparing Figure 12 and 15.

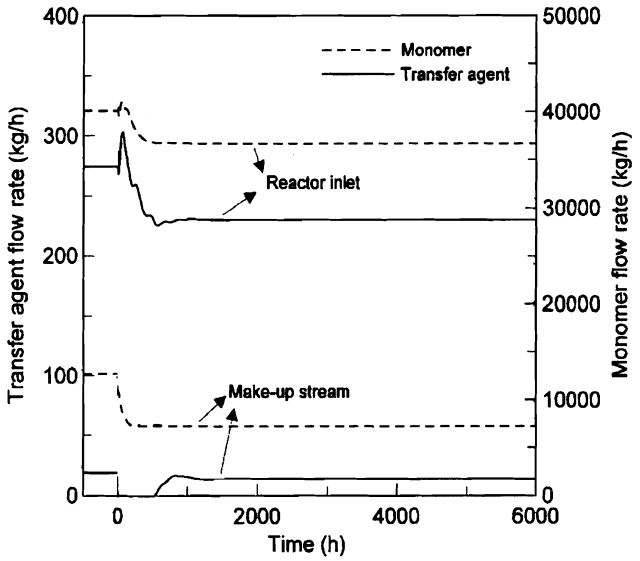

Figure 14. Monomer and transfer agent flow rates during grade transition for the reactor with recycle. Make-up flow rates are manipulated by PI controllers.

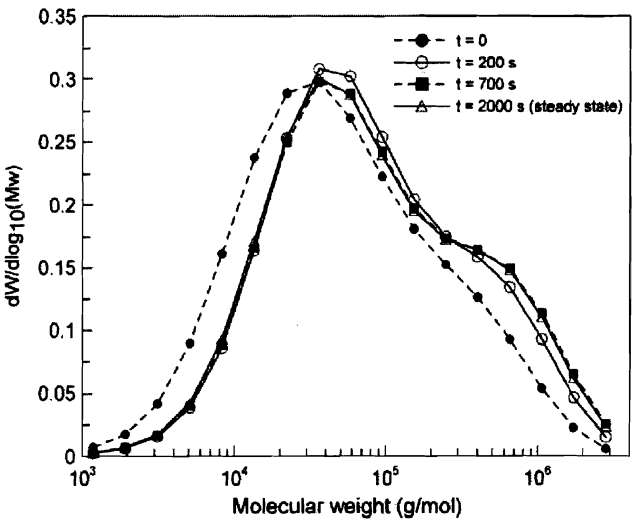

Figure 15. MWD at the reactor exit during grade transition for the reactor with recycle. Make-up flow rates are manipulated by PI controllers.

Conclusion

A comprehensive dynamic model of the high-pressure polymerization of ethylene in tubular reactors was developed. The model, which considers variable physical and transport properties calculated by means of rigorous correlations, can predict the full MWD, monomer conversion, reactants concentrations, average molecular weights and average degree of branching along the axial distance and time. In particular, the pgf technique allowed easy and efficient modeling of the full MWD in spite of the reactor model complexity. The results obtained show that the model has great potential for analyzing the dynamic

responses of MWD and other process variables under different transition policies, as well as in predicting the influence of process perturbations and for studying start-up and shut-down operations. The influence of the material recycle on the process dynamics was assessed. In particular, it was shown that the recycle stream must be taken into account when analyzing transition policies. It was also shown that a significant improvement can be obtained by optimizing the transition procedure.

When MWD prediction is included in a polymerization model, the size of the model is strongly determined by the number of predicted points of the MWD. The modeling approach presented in this work has advantageous features for optimization applications, since the pgf technique provides the possibility of tailoring the size of the model, since it allows the calculation of only an arbitrarily selected set of points of the MWD without loss of accuracy.

Nomenclature

A_j Coefficients in Stehfest's algorithm [Equation (30)]
C_j Molar concentration of the jth component
Cp Heat-capacity of the reaction mixture
Cp_M Monomer heat-capacity
Cp_p Polymer heat-capacity
D Reactor internal diameter
D_e Reactor external diameter
f_{ik} Initiation efficiency of fictitious initiator k, ($k = 1, 2$)
f_o Efficiency of inert generation by oxygen
h_j Internal heat transfer coefficient
h_j Jacket heat transfer coefficient
I_k kth fictitious peroxide initiator, ($k = 1, 2$)
k Thermal conductivity of the reaction mixture
k_{bb} Back-biting rate constant
k_β Tertiary radical β-scission rate constant
$k_{\beta 1}$ Secondary radical β-scission rate constant
k_{ik} Initiation rate constant of the kth fictitious initiator, ($k = 1, 2$)
k_{mi} Monomer initiation rate constant
k_o Initiation by oxygen rate constant
k_p Propagation rate constant
k_{tc} Termination by combination rate constant
k_{tdt} Thermal degradation rate constant
k_{trm} Transfer to monomer rate constant
k_{trp} Transfer to polymer rate constant
k_{trs} Transfer to transfer agent rate constant
k_w Thermal conductivity of the reactor wall
L Reference reactor length
LCB Long-chain branching
M Ethylene monomer
Me Methylene group
$\overline{M}_n$ Polymer number average molecular weight
$\overline{M}_w$ Polymer weight average molecular weight
$\overline{M}_{wj}$ Molecular weight of the jth component
n_i Number fraction of molecules with i monomeric units
O_2 Oxygen
P Reactor pressure
$P(m)$ Polymer molecule of chain length m, ($m = 1, \ldots, \infty$)
$R(m)$ Living radical of chain length m, ($m = 0, \ldots, \infty$)
R_f Fouling resistance
r_j Net generation rate of the jth component
r_{pm} Reaction rate of the propagation reaction
S Fictitious transfer agent
SCB Short chain branching
t Reaction time
T Reactor temperature
T_j Jacket temperature
U Overall heat-transfer coefficient
v Axial velocity
Vi Vinyl group
Vd Vinylidene group
w_i Weight fraction of molecules with i monomeric units
w_M Monomer weight fraction
w_S Transfer agent weight fraction
w_X Inert species weight fraction
X Inert molecule.
z Axial length

Greek Symbols

ΔH Global heat of reaction
$\phi_{a,l}$ Probability generating function (pgf) of the radical chain length distribution. Subscript $a = 0, 1, 2$ stands for the MWD expressed in number, weight and chromatographic (mass times the molecular weight) fraction, respectively; subscript l is the dummy variable of the pgf
$\varphi_{a,l}$ Probability generating function (pgf) of the polymer chain length distribution. Subscripts a and l have the same meaning as for $\phi_{a,l}$
λ_a ath order moment of the radical chain length distribution
η Viscosity of the reaction mixture
μ_a ath order moment of the polymer chain length distribution
ρ Density of the reaction mixture
ρ_M Monomer density
ρ_p Polymer density

Acknowledgements: The authors wish to thank *CONICET (National Research Council of Argentina), ANPCyT (National Agency for Scientific and Technological Promotion, Argentina)*

Macromol. React. Eng. **2009**, *3*, 398–411

Macromolecular Journals
DOI: 10.1002/mren.200900013

and *UNS* (*Universidad Nacional del Sur*, Bahía Blanca, Argentina) for financial support.

Received: February 2, 2009; Revised: May 1, 2009; Accepted: May 11, 2009; Published online: July 10, 2009; DOI: 10.1002/mren.200900013

Keywords: dynamic model; molecular weight distribution; polyethylene (PE); probability generating function; tubular reactor

[1] A. Brandolin, M. H. Lacunza, P. E. Ugrin, N. J. Capiati, *Polym. React. Eng.* **1996**, *4*, 193.
[2] C. Kiparissides, G. Verros, G. Kalfas, M. Koutoudi, C. Kantzia, *Chem. Eng. Commun.* **1993**, *121*, 193.
[3] M. H. Lacunza, P. E. Ugrin, A. Brandolin, N. J. Capiati, *Polym. Eng. Sci.* **1998**, *38*, 992.
[4] C. Kiparissides, A. Baltsas, S. Papadopoulos, J. Congalidis, P. J. Richards, R. M. Kelly, B.Y. Ye, *Ind. Eng. Chem. Res.* **2005**, *44*, 2592.
[5] V. M. Zavala, L. Biegler, *Ind. Eng. Chem. Res.* **2006**, *45*, 7867.
[6] M. Asteasuain, P. E. Ugrin, M. H. Lacunza, A. Brandolin, *Polym. React. Eng.* **2001**, *9*, 163.
[7] N. Agrawal, G. P. Rangaiah, A. K. Ray, S. K. Gupta, *Chem. Eng. Sci.* **2007**, *62*, 2346.
[8] M. Asteasuain, A. Brandolin, *J. Appl. Polym. Sci.* **2007**, *105*, 2621.
[9] M. Asteasuain, A. Brandolin, *Comput. Chem. Eng.* **2008**, *32*, 396.
[10] A. Brandolin, E. M. Valles, J. N. Farber, *Polym. Eng. Sci.* **1991**, *31*, 381.
[11] C. Kiparissides, G. Verros, J. F. MacGregor, *J. Macromol. Sci., Rev. Macromol. Chem. Phys.* **1993**, *C33*, 437.
[12] C. Kiparissides, G. Verros, A. Pertsinidis, *Chem. Eng. Sci.* **1994**, *49*, 5011.
[13] H. Mavridis, C. Kiparissides, *Polym. Process Eng.* **1985**, *3*, 263.
[14] C. Kiparissides, G. Verros, A. Pertsinidis, *AIChE J.* **1996**, *42*, 440.
[15] D. Kim, P. D. Iedema, *Chem. Eng. Sci.* **2004**, *59*, 2039.
[16] C. Schmidt, M. Busch, D. Lilge, M. Wulkow, *Macromol. Mater. Eng.* **2005**, *290*, 404.
[17] M. Häfele, A. Kienle, M. Boll, C. U. Schmidt, *Comput. Chem. Eng.* **2006**, *31*, 51.
[18] M. Asteasuain, S. M. Tonelli, A. Brandolin, A. Bandoni, *Comput. Chem. Eng.* **2001**, *25*, 509.
[19] A. Cervantes, S. M. Tonelli, A. Brandolin, A. Bandoni, L. Biegler, *Comput. Chem. Eng.* **2000**, *24*, 983.
[20] M. Mummudi, R. O. Fox, *J. Chin. Inst. Chem. Engrs.* **2006**, *37*, 1.
[21] V. M. Zavala, L. T. Biegler, *Comput. Chem. Eng.* **2009**, *33*, 379.
[22] M. Asteasuain, S. Pereda, M. H. Lacunza, P. E. Ugrin, A. Brandolin, *Polym. Eng. Sci.* **2001**, *41*, 711.
[23] M. Asteasuain, C. Sarmoria, A. Brandolin, *Polymer* **2002**, *43*, 2513.
[24] M. Asteasuain, C. Sarmoria, A. Brandolin, *Polymer* **2002**, *43*, 2363.
[25] A. Brandolin, M. Asteasuain, C. Sarmoria, A. R. López, K. S. Whiteley, B. del Amo Fernández, *Polym. Eng. Sci.* **2001**, *41*, 1156.
[26] M. Asteasuain, Doctoral Thesis, Universidad Nacional del Sur, Bahía Blanca, Argentina, 2003.
[27] A. Brandolin, Doctoral Thesis, Universidad Nacional del Sur, Bahía Blanca, Argentina, 1987.
[28] C. H. Chen, J. G. Vermeychuk, S. A. Howell, P. Ehlrich, *AIChE J.* **1976**, *22*, 463.